



# Ice rose diagrams for probabilistic characterization of the ice drift behavior in the Beaufort Sea

Chana Sinsabvarodom<sup>a,\*</sup>, Wei Chai<sup>b,\*\*</sup>, Bernt J. Leira<sup>a</sup>, Knut V. Høyland<sup>c</sup>, Arvid Næss<sup>d</sup>

<sup>a</sup> Department of Marine Technology, Norwegian University of Science and Technology, Norway

<sup>b</sup> School of Naval Architecture, Ocean and Energy Power Engineering, Wuhan University of Technology, China

<sup>c</sup> Department of Civil and Environmental Engineering, Norwegian University of Science and Technology (NTNU), 7491, Trondheim, Norway

<sup>d</sup> Department of Mathematical Sciences, Norwegian University of Science and Technology, Norway

## ARTICLE INFO

### Keywords:

Ice rose  
Ice drift  
Ice thickness  
Probabilistic analysis

## ABSTRACT

The purpose of the present paper is to investigate the viability of the so-called ice rose diagram, which is a graphic tool to provide a succinct view of the ice drift information such as speed and direction of ice drift events in terms of their relative distribution at a local observation station to support the dynamic ice-structure interaction in cold regions. The ice drift data is collected by using local subsurface measurements based on acoustic Doppler current profilers (ADCP) in the Beaufort Sea during 2006–2017. Probabilistic analyses are performed in order to characterize the time-series data from these ADCP measurements. Both the ice drift speed and direction are treated as random variables for which analytical probability density functions are fitted. It is found that sea ice in the Beaufort Sea tends to drift at a lower speed during the winter season (i.e. the growth season) than during the summer season (i.e. the melting season). The Weibull distribution provides the most appropriate fit to the data of ice drift speeds during the growth season. For the melting season, a mixed distribution provides the most appropriate fit for the drift speed. Regarding directionality of the ice drift, a mixed Von Mises distribution is applied in order to represent its statistical properties. In this work, the relationship between ice drift speed and wind speed is also studied. It is found that the magnitude of the ice drift speed is approximately 2.5% of the wind speed during the winter season.

## 1. Introduction

The understanding of ice conditions is crucial for safe design and operation of offshore structures in Polar regions because sea ice and the induced ice loads represent a main challenge for offshore operations in cold regions. The drift of sea ice is caused by disturbances from the surrounding environment. Typically, the external forces acting on the sea ice caused by the surrounding environment can be split into five components: the air stress at the air-ice interface, the water stress at the water-ice interface, the ice-ice contact stress, the Coriolis force and the pressure gradient force due to tilting of the water surface (Campbell, 1965; Leppäranta, 2011). Among these driving forces, the air stress due to wind and the water stress due to the ocean current are the major components when it comes to driving the sea ice motion process.

Typically, a sea ice kinematic model based on a mathematical description of the two-dimensional motion of a rigid body is applied for

the ice drift. Extension to a stochastic modelling of the ice drift is also frequently made. Sea ice kinematic can be applied in the propose of the ice drift mapping. The observation of the ice drift kinematic in the ocean can be investigated based on three different methodologies which are the Lagrangian, Eulerian and imaging (remote sensing) approaches. Traditionally, sea ice kinematics is mapped by using drifters, buoys or research stations anchored into the ice (Leppäranta, 2011). This corresponds to the Lagrangian approach, where the pathways of the ice floes are monitored in order to observe their kinematic behaviour. Whereas in the Eulerian approach, the instantaneous kinematic properties are observed at a fixed point in space at a specific location (Li and Lam, 1964).

GPS tracking can be installed at the ice floes and icebergs to observe the drift motion. (Yulmetov et al., 2016). It provides the pathways of ice drift and the kinematic properties corresponding to the Lagrangian approach. Whereas, the local monitoring is an alternative to observation

\* Corresponding author.

\*\* Corresponding author.

E-mail addresses: [chana.sinsabvarodom@ntnu.no](mailto:chana.sinsabvarodom@ntnu.no) (C. Sinsabvarodom), [chaiwei@whut.edu.cn](mailto:chaiwei@whut.edu.cn) (W. Chai).

of the sea ice drift in a specific area. Typically, underwater mooring buoys (Belliveau et al., 2001) are employed in order to record the ice thickness, drift speed, temperature, water pressure, etc. Generally, the upward looking acoustic Doppler current profile (ADCP) instrument is installed at the top of mooring buoy in order to observe the ice motion (Birch et al., 2000; Visbeck and Fischer, 1995). For the aerial image, Satellites are commonly used to investigate the climate at larger scales. The information from satellites consists of various types of data such as ice concentration, ice thickness, ice drift speed, etc. in the view of an aerial image. The data generally covers quite large areas, while on the other hand the data is not characterized by a very high precision level. However, machine learning algorithms can be applied to estimate the ice thickness from the Satellite images (Shamshiri et al., 2022).

For more than a century, the atmospheric drag has been identified as the main driver of ice drift (Nansen, 1902). As a rule of thumb, the wind-driven ice drift speed is 2–3% of the wind speed on the average, and the drift direction deviates by 30° to the right or the left relative to the wind direction (depending on whether a location on the Northern or South hemisphere is considered, due to the Coriolis force (Leppäranta, 2011)). The percentwise magnitude of ice drift speed relative to the wind speed is generally assumed to hold both for the Arctic and the Antarctic (Alberello et al., 2020). In the central Arctic, Spreen et al. (2011) studied the velocity of ice drift based on satellite measurements. They found that wind is the major influencing factor in relation to ice drift in this region. The drift speed of the ice cover is approximately two to three percent of the mean wind speed at 10 m above the water surface during the winters (October–May) from 1992/1993 to 2008/2009. On time scales from days to months, more than 70% of the variance of the ice motion is described by the geostrophic wind alone (Thorndike and Colony, 1982). In Subarctic regions, the wind-induced drift due to the atmospheric circulation causes exchange of sea ice between the Kara Sea and the Central Arctic Ocean (Vinje and Kvambekk, 1991).

The ice condition can be classified as being thin, medium and thick based on a combination of the ice thickness and the ice concentration, which are both important in order to characterize the physical properties in term of mass and volume which are being input to the ice drift model. The ice concentration generally also has implications with respect to the type and appearance of the ice (Alberello et al., 2020; Løset et al., 2006; McPhee, 1980; WMO, 1970). The ice concentration (fraction of areal coverage of ice) is another key parameter, it more or less determines if the ice drift is free, or if energy is consumed by ice deformation (ice-ice contact stress). When the sea ice cover is loose or comprised of multiple floes, the internal sea ice stresses are negligible (Alberello et al., 2020). The free drift is a good approximation for individual, separate ice floes and for fields with low compactness (i.e. the ice concentration is less than about 0.8) (Leppäranta, 2011). An often quoted threshold for ridging and rafting is 0.8. In general, the three characteristic values represented by ice concentration, ice thickness and ice drift speed are of key importance in any study related to ice drift for cases with low ice concentration (Løset et al., 2006).

The changing climate and the resulting declining extent of the sea ice has led to a significant increase of offshore activities in the Arctic region (Xu et al., 2021). Ice drift velocity and direction are key parameters in a range of applications, spanning from climate models to different types of engineering projects. For the design and operation of ships, fixed and floating marine structures ice velocity has important consequences. Fixed structures respond differently for different ice velocities and for certain combinations of ice drift velocity and thickness dangerous resonant vibrations may occur, and safe and realistic estimation of ice-induced fatigue requires a realistic ice drift distribution. During the operation with a floating structure (for example loading of oil) the ice drift direction needs to be predictable, a change in ice drift direction during the operation may cause problems. For both short and long term planning of ship routing it is important to quantify the ice drift, the ship will sail slower and use more fuel when sailing against the ice drift. Furthermore, the mass and drift velocity of sea ice can be considered as

the momentum to estimate the ice management efficiency, which can be observed from the tension in mooring line system during the vessel stationary keeping in ice (Sinsabvarodom et al., 2020, 2021a). Change of ice drift direction in the Arctic takes place frequently and the drift direction can be completely reversed even on a time scale of a few hours (Rossiter and McKenna, 2013).

The focus of the present study is to generate the ice rose diagram in order to conveniently provide information about ice drift speed magnitude and relative distribution of ice drift direction in the Beaufort sea. The so-called rose diagram was originally applied for wind speed analysis in order to display information about the distribution of the wind direction and the wind speed (Zelenko and Lisac, 1994). It was found that the probability density function (PDF) of the wind directions inherently contains several peaks corresponding to several characteristic directions. Therefore, mixed statistical models are applied in order to cope with these multi-peak features. Kawaguchi et al. (2019) studied the characteristics of sea ice conditions in the Beaufort sea. Ice rose histograms were applied in order to display the ice drift properties in connection with ocean currents around the local measurement station in the Northwind Abyssal Plain (NAP).

In this work, the ice data is collected by ADCP instruments installed at local mooring stations as part of Beaufort Gyre exploration project carried out by the Woods Hole oceanographic institution. The ice drift data is here employed in order to establish the so-called ice rose diagrams, which are based on a probabilistic assessment of the ice drift speeds. The year-round time series of the ice drift in the different years are treated as random variable, which allows a probabilistic analysis of the ice drift speed and direction also accounting for the seasonal variations.

## 2. Locations of mooring buoys in the Beaufort Sea

For development of the ice rose diagrams in the Beaufort Sea, utilization was made of measurements from underwater mooring buoys installed in the Beaufort Gyre region in order to observe the behavior of sea ice. The present study employs the data obtained in the Beaufort Gyre exploration project organized by Woods Hole oceanographic institution, which is publicly available online (<http://www.whoi.edu>). Four stations with bottom-tethered moorings were installed on the seabed at the four locations illustrated in Fig. 1. The four stations represent an Eulerian grid, which fixed points located on the seabed in order to record the global ice drift in the Beaufort Sea. Information about the relevant measurement site locations and the period of available data records for each station is listed in Table 1.

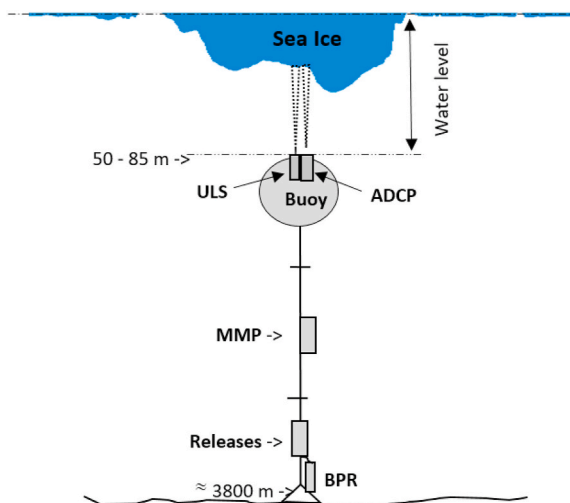
The mooring buoy at each station is equipped with four instruments: the upwards looking sonars (ULS), acoustic Doppler current profilers (ADCP), the bottom pressure recorders (BPR) and the McLane moored profilers (MMP) (Richard and Andrey, 2006; Richard et al., 2003) as illustrated in Fig. 2. These instruments are recording different types of physical properties, i.e. the BPR is employed in order to measure the pressure at the bottom of the sea bed. The MMP is deployed in order to profile the temperature and the salinity of the surrounding water at each station. The Acoustic Doppler Current Profiler (ADCP) is a sonar device, which transmits acoustic signals at a fixed frequency (600 kHz) with a bin size of 2m and with 25 depth bins that record the reflections by the sea ice. The return echo signal is received by the ADCP and is subsequently transformed into an ice velocity. The upward-looking sonar (ULS) is deployed in order to observe the draft of the sea ice cover with a resolution of approximately  $\pm 10$  cm for sea wave conditions and  $\pm 5$  cm for the case with no disturbance from sea waves. More details about the ADCP and ULS equipment, data processing and device resolution are given in (<https://www2.whoi.edu/site/beaufortgyre/data/mooring-data/mooring-data-description/>) and in Richard and Andrey (2006), respectively. The number of data points in the measurement record for the different year is given in the link (<https://www2.whoi.edu/site/beaufortgyre/data/mooring-data/>)



Fig. 1. Sites for collection of data in the Beaufort Gyre region in the Beaufort Sea, the red spots on the map represent the relevant locations (<https://earth.google.com/web/>). (For interpretation of the references to color in this figure legend, the reader is referred to the Web version of this article.)

Table 1  
Location and data records of measurement stations.

Station	Latitude	Longitude	Water depth (m)	Available data (year)											
				2006 - 2007	2007 - 2008	2008 - 2009	2009 - 2010	2010 - 2011	2011 - 2012	2012 - 2013	2013 - 2014	2014 - 2015	2015 - 2016	2016 - 2017	
A	75 0.0270°N	149 59.9659°W	3825	-	-	-	-	✓	✓	-	✓	✓	✓	✓	
B	77 59.8615°N	149 57.6695°W	3821	-	-	-	-	✓	✓	✓	✓	✓	✓	-	
C	76 59.063°N	139 57.222°W	3722	-	-	-	-	-	-	-	-	-	-	-	
D	74 0.0007°N	140 0.0606°W	3521	✓	✓	✓	✓	✓	✓	✓	✓	✓	✓	✓	



Subsurface mooring buoy redeployment at site location  
[Photo by Peter Lourie, October 4, 2016]

Fig. 2. Illustration of observational mooring system and the positions of the apparatus (<https://www2.who.edu/site/beaufortgyre/data/mooring-data/>).

### 3. Theoretical background

In this section, methods for analysis and characterization of ice drift behavior are presented. The magnitude and direction of the ice drift are estimated from its velocity components, which were monitored by means of the ADCP equipment. Subsequently, the velocity vectors in the horizontal plane are employed in order to generate the so-called ice rose diagram. For the purpose of a probabilistic assessment, various types of statistical models are considered in order to describe the seasonal behavior of ice drift speed and direction.

#### 3.1. Calculation of horizontal ice drift speed and direction

Inherently, the random speed and direction of the ice drift are caused by the external forces which originate from the immediate environment. The primary data from the ADCP measurement provides the vector components of the ice drift velocity during each hour,  $t$ , referred to a three-dimensional earth-based coordinate system in the terms of north-south, east-west, and up-down with origin above the respective observation. The magnitude of the ice drift speed,  $u_h(t)$  in the horizontal direction is expressed by equation (1):

$$u_h(t) = \sqrt{u_N(t)^2 + u_E(t)^2} \quad (1)$$

Where  $u_N$  and  $u_E$  are the horizontal velocity vectors in the latitude (N) and longitude directions (E), respectively. The direction of ice drift is specified in terms of rotation angle,  $\theta$ , corresponding to a polar coordinate system with origin at the observation station. The rotational angle can obtain values in the range from 0 to 360°. It is calculated based on the components of the velocity vector, i.e.  $u_N$  and  $u_E$ , as given in equation (2):

$$\theta = \arctan\left(\frac{u_E}{u_N}\right) \quad (2)$$

##### 3.1.1. The general equation of ice drift

The general equation describing sea ice motion comprises five different forcing terms which are the following, i.e the wind-induced stress at the air-ice interface,  $\tau_{air}(t)$ , the stress at the water-ice interface,  $\tau_{water}(t)$ ; the Coriolis force,  $\rho_i \cdot h_i \cdot f \cdot u_h(t)$ , the pressure gradient force due to tilting of the water surface on which the ice floats,  $G(t)$  and the stress transmission or the internal ice stress,  $R(t)$  (Campbell, 1965; Lepäranta, 2011; McPhee, 2008). Therefore, the general equation of motion for the ice drift can be expressed as:

$$\rho_i \cdot h_i \cdot \left( \frac{du_h(t)}{dt} + f \cdot u_h(t) \right) = \tau_{air}(t) + \tau_{water}(t) + G(t) + R(t) \quad (3)$$

Where,  $\rho_i$  is the sea ice density,  $h_i$  is the thickness,  $f$  is the Coriolis parameter. If equilibrium conditions corresponding to a steady flow is considered, the acceleration of the sea ice can be assumed to be negligible. Accordingly, by setting the acceleration term in equation (3) equal to zero, this simplifies into equation (4):

$$\tau_{air}(t) + \tau_{water}(t) + D(t) + G(t) + R(t) = 0 \text{ where, } D(t) = -\rho_i \cdot h_i \cdot f \cdot u_h(t) \quad (4)$$

Nansen (1902) studied the ice drift behavior corresponding to free drift conditions by neglecting the internal ice stress and the gradient current terms. Consequently, equation (4) can be rewritten as

$$\tau_{air}(t) + \tau_{water}(t) + D(t) = 0 \quad (5)$$

Rossby and Montgomery (1935) assumed that the thickness of the sea ice can be set equal to zero in order to neglect the inertia force and the Coriolis force. Subsequently, equation (5) can be reduced into equation (6). This provides a good quantitative agreement with observations of the air stress and the ice velocity.

$$\tau_{air}(t) + \tau_{water}(t) = 0 \quad (6)$$

According to the quadratic drag formulation (Lepäranta, 2011), the air and water stress can be expressed in vector form as

$$\tau_{air} = \rho_{air} \cdot C_{air} |U_{air}| \exp(i\theta_{air}) \cdot U_{air} \quad (7)$$

$$\tau_{water} = \rho_{water} \cdot C_{water} |(U_{water} - u_h)| \exp(i\theta_{water}) \cdot (U_{water} - u_h) \quad (8)$$

where  $C_{air}$ ,  $C_{water}$ ,  $\theta_{air}$  and  $\theta_{water}$  denote air drag coefficient, water drag coefficient, turning angle in atmosphere and turning angle in water, respectively. From equations (6)–(8), the ice drift velocity, based on free drift of thin ice, can be expressed as

$$u_{ice} = Na \cdot \exp[-i\theta_0] \cdot U_{air}(t) + U_{water} \quad (9)$$

where  $Na = \sqrt{\rho_{air} \cdot C_{air} / \rho_{water} \cdot C_{water}}$  is called the Nansen number, which is the normalization between ice-air stress and the ice-ocean velocity difference remains. Typically, the wind velocity is naturally scaled by the Nansen number down to  $Na \cdot U_{air}$  for a representative wind-driven ice velocity. The ratio of  $C_{air}/C_{water}$  is the key parameter to determine the free drift speed. The value is not very sensitive to the type of ice. The deviation angle,  $\theta_0$  is  $\theta_{water} - \theta_{air}$ . If other terms are small, the ice drift velocity in equation (9) can be written as expressed by equation (10). The direction between  $|u_h - U_{water}|$  and  $U_{air}$  depends on the boundary-layer angle.

$$Na \cdot U_{air} \approx |u_h - U_{water}| \quad (10)$$

The values for  $Na$  depend on the geographical region and typical values are in the from 1.7% to 3.5% for the free drift condition (Lepäranta, 2011). In the present work, the horizontal wind speed,  $U_{air}$  is obtained from the Ventusky web application and the ice drift speed,  $u_h$  is calculated from the horizontal speed in equation (1) based on the ADCP measurements.

#### 3.2. Correcting for open water events

The ice draft data is collected from upward looking sonars (ULS) at an interval of 2 s, which is a much more frequent logging than for the ADCP data. Therefore, the time interval of the ADCP data is applied as the main time increment. The ice draft data from the ULS measurements at the same time instants are employed in order to perform the statistical analysis.

The resolution of the apparatus for the ULS measurements is approximately  $\pm 5$ –10 cm. For open-water (or thinnest ice) measurement, the error of the ULS instruments is corrected by considering the uncertainty of beta (the sound speed). Identification of open-water events based on the ULS measurements becomes more difficult when the water surface is disturbed by waves. The effect of water surface tilting reduces the resolution of the ULS measurement, and the error related to the ice draft estimation may approach  $\pm 10$  cm. In calm water, the error associated with identification of open water is estimated to be approximately  $\pm 5$  cm. Further details related to the resolution for the ULS measurements in the Beaufort Gyre exploration project are given in Richard and Andrey (2006). When open water is identified based on the ice draft from the ULS measurement being zero, the corresponding point in the ADCP drift speed record is removed (Richard and Andrey, 2006). The procedure for identification of open water versus ice cover is illustrated in Fig. 3.

#### 3.3. Correlation coefficient

The correlation between two random variables can be described by the correlation coefficient. In the present study, the covariation between the ice drift speed and the ice thickness is quantified by means of the correlation coefficient,  $\rho$ , as expressed in equation (11). The values of the ice thickness are obtained from ice draft measurements obtained by the ULS equipment.

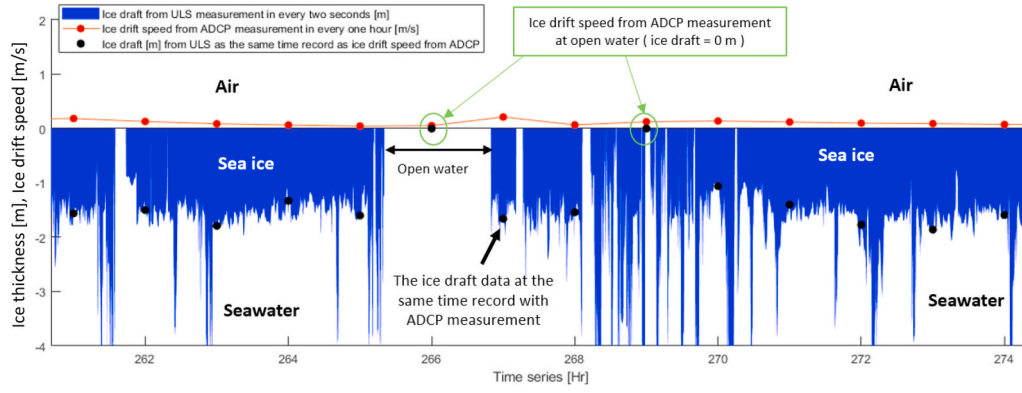


Fig. 3. An example of sea ice classification for open waters by using time series from both ULS and ADCP measurements.

$$\rho = \frac{\sum (h_i - \bar{h}_i)(u_h - \bar{u}_h)}{\sqrt{\sum (h_i - \bar{h}_i)^2 \sum (u_h - \bar{u}_h)^2}} \quad (11)$$

where,  $h_i$  and  $\bar{h}_i$  correspond to the observed ice thickness and the mean value of the ice thickness during each season,  $u_h$  and  $\bar{u}_h$  correspond to the horizontal speed and the mean value of the horizontal speed during each season.

### 3.4. Wind speed and ice drift speed data

For this research, the wind speed data was obtained from the Ventusky web application, which has been developed by the company InMeteo. This web application is a platform for weather prediction and visualization of meteorological data at a global scale (<https://www.ventusky.com/>). A numerical model for weather prediction has been developed by the Canadian Meteorological Centre, CMC. Usually, the calculations are performed every 3 h with a grid resolution of roughly 25 km. The data is updated in every 12 h and the web application has been available since 2016. The wind speed at 10 m above the water surface at the ADCP measurement stations are employed in order to study the joint variation of the wind and ice drift speeds. The data points for the ice drift speed that coincide in time with the more sparse data points for the wind speed are selected as a basis for the analysis as illustrated in Fig. 4. Data records obtained from ADCP measurement in the year 2016–2017 were available only for stations A and D, and the distance between these two stations is approximately 316.8 km.

### 3.5. Mixed statistical models

Due to the complexity of the ice drift phenomenon, the empirical histograms that can be obtained from the measurements may exhibit several distinct peaks, which cannot be described by simple probabilistic models. The aim of this section is to briefly describe mixed statistical models, which are suitable for representation of multi-peak density

functions such that the complex nature of the random ice drift can be adequately represented. The mixed statistical models are more efficient and flexible in order to fit arbitrary histogram shapes which are obtained based on the available data sets (Wang et al., 2012). The mixed distributions can be exemplified by the so-called bimodal, skewed and heavy tail distributions as illustrated in Fig. 5. The pdf of the mixed distributions are obtained by means of a weighted summation of a number parent pdfs as given in equation (12).

$$f_{pmf}(x) = \sum_{i=1}^n w_i f_i(x) = w_1 f_1(x) + \dots + w_i f_i(x) + \dots + w_n f_n(x) \quad (12)$$

where,  $w_i$  denotes the non-negative weight factors, which sum to one as given by equation (13), the pdfs,  $f_i(v_h)$ , belong to the “classical” probabilistic families such as the normal distribution, the log normal distribution, the exponential distribution, the gamma distribution, the Weibull distribution and the Von Mises distribution etc.

$$w_i > 0 \quad \text{and} \quad \sum_i w_i = 1. \quad (13)$$

### 3.6. The Von Mises distribution

The Von Mises distribution is a continuous function which is suitable for statistical characterization in the circular domain. It is basically different from probability distributions with unbounded domains of definition. The pdf is defined in polar coordinates within the interval from 0 to 360°. This type of distribution has been widely used e.g. for characterization of wind and wave directions (Carta et al., 2008). Furthermore, it can be applied as a component of the mixed distributions that were described in the previous sections. In the present study, the Von Mises distribution is applied in order to represent the statistical properties of ice drift direction. The pdf is expressed by equation (14) as:

$$f_{vM}(\theta) = \frac{1}{2\pi I_0(\kappa_i)} \exp \left[ \kappa_i \cos \left( \frac{\pi}{180} \theta - \mu_i \right) \right] \quad (14)$$

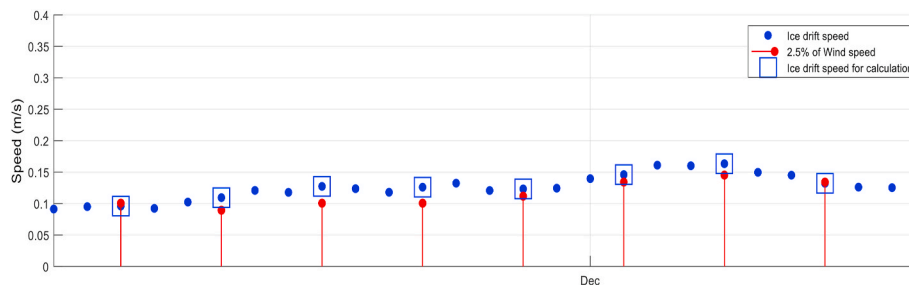


Fig. 4. Selection of data points for ice drift speed for the purpose of estimating the wind and ice drift speed relationship. (Wind speed sampling rate, 3 h; Ice drift speed sampling rate, 1 h)

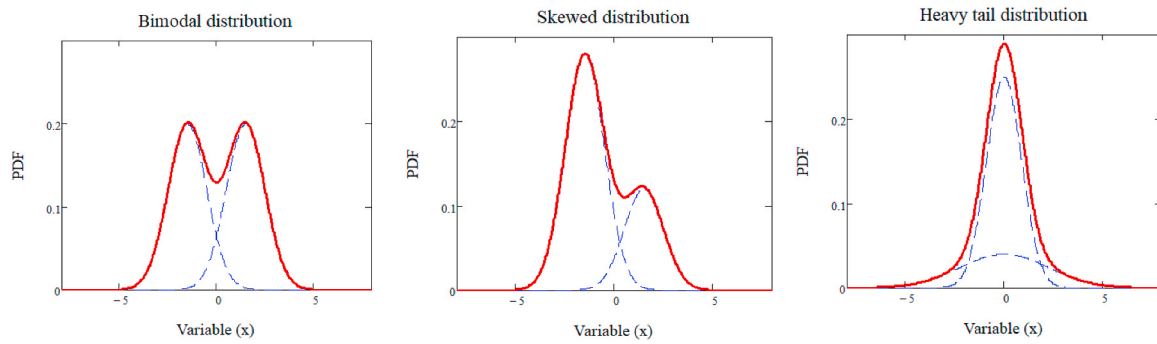


Fig. 5. Examples of probability densities corresponding to mixed statistical models.

where  $\kappa_i \geq 0$ ,  $0^\circ \leq \theta < 360^\circ$  and  $0 \leq \mu_i \leq 2\pi$  are the shape parameter and the location parameter of the Von Mises distribution, respectively.  $\theta$  is the random angle, which is calculated from equation (2).  $I_0(\cdot)$  is the modified Bessel function of the first kind and zero order as given in equation (15).

$$I_0(\kappa) = \sum_{l=0}^{\infty} \frac{\kappa^{2l}}{2^{2l}(l!)^2} \tag{15}$$

In this research, the procedure of the analysis starts from obtaining time series data of ice drift velocity and ice thickness from ADCP and ULS measurements. After that, the classification of the ice cover is applied to distinguish between the presence of ice versus open water. Calculation of ice drift speed and direction is required in order to interpret the collected time-series which are obtained as a result of the measurements. The seasonal dependence of ice drift behavior for the growth season versus the melting season is investigated. Subsequently, generation of the ice rose diagram as well as probabilistic assessment are performed as illustrated in Fig. 6.

4. Result

The ice drift data is collected from ADCP measurements at an interval of 1 h. Data at three stations is available: A, B, D. For station C, no data can be obtained. The Eulerian approach corresponds to monitoring of the velocity of the ice drift at fixed points in space. The ice data record starts on 1st October each year, based on the specified time for start of the winter season according to the Canadian regulations. The ADCP measurements provide the velocity components in three orthogonal

directions. The calculation of horizontal ice drift speed is carried out by means of equation (1). The long-term data of ice drift time series was used in the analysis. The ice drift speeds measured at the three stations during 2013–2014 are shown in Fig. 7. Owing to the different time intervals for the records from the ULS and ADCP measurements, data points of ice thickness at the same time instants as those available for the ice drift speed are selected in order to perform the analysis as illustrated in Fig. 8.

Examples of a satellite images during the highest-level ice thickness before going into the melting season are shown in Fig. 9. In this analysis, the drifting ice with a certain ice thickness is considered as the parametric constraint for the analysis. The same time recorded data of ice drift speed is removed when the ice thickness equals zero because it is considered to represent ice-free data or open water data. The open water around the observational area is demonstrated in Fig. 10.

4.1. Ice condition and influence of seasonal effects on the ice drift

Due to the random variation of the environmental conditions with time the ice drift characteristics also exhibit a similar behaviour. Accordingly, a statistical representation of the variability of the ice conditions (i.e. ice thickness, ice concentration, ice type, etc.) as well as the ice drift in a given climate becomes most relevant (Leppäranta, 2011). In present study, the seasonal effect on ice drift speed is clearly observed from the time series of ice drift speed amplitude shown in Fig. 7. The sea ice drift velocity decreased when the ice started to form (October and November), reached a somewhat constant level for the rest of the winter, increased at the onset of melting (June) and then stabilized over the summer. The ice thickness increased steadily the entire

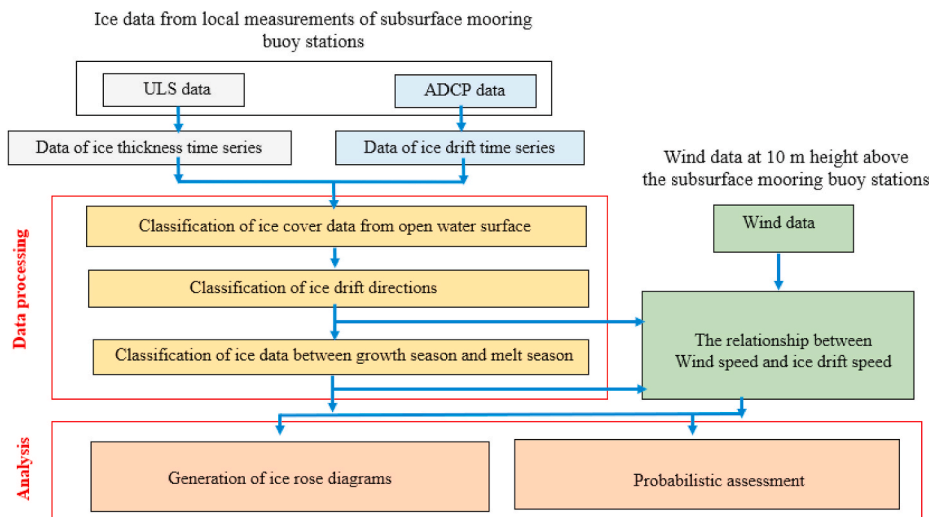


Fig. 6. Flowchart of the steps required for development of the ice rose diagram as well as probabilistic assessment of wind speed and ice drift speed.

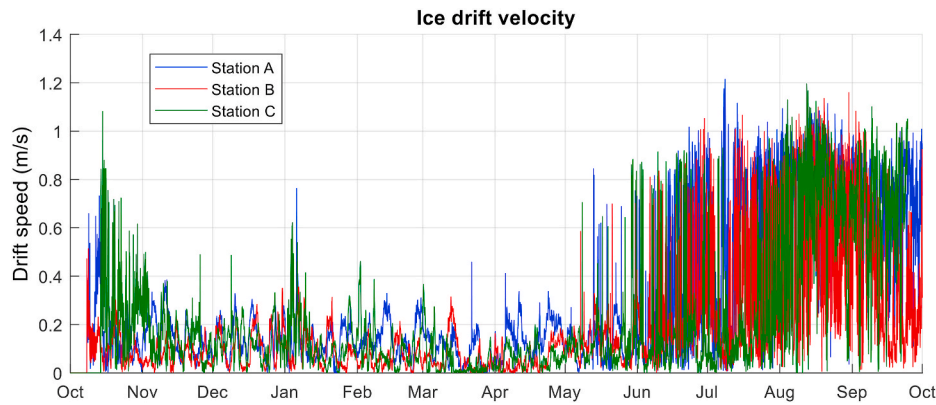


Fig. 7. Time series of ice drift speed during 2013–2014 obtained from the ADCP measurement.

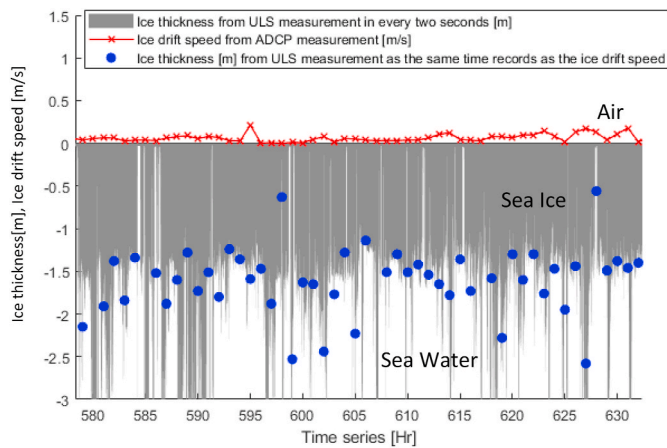


Fig. 8. Illustration of data extraction for ice thickness (ULS sampling rate, 2 s; ADCP sampling rate, 1 h).

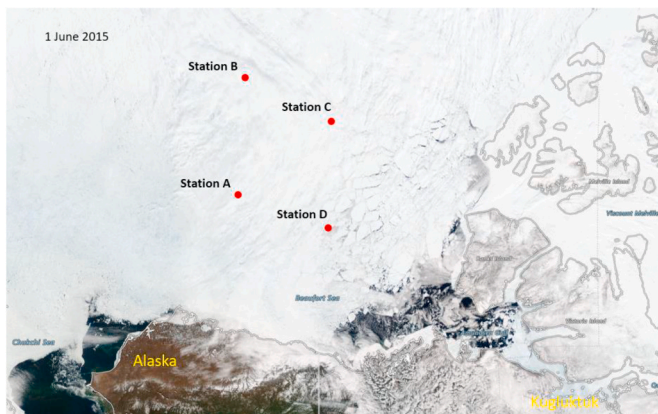


Fig. 9. Satellite image of the area with the observational stations on June 1, 2015 (<https://zoom.earth/>).

winter (October–May) and decreased again from June/–July as illustrated in Fig. 11. It seems to be correlated with drift velocity during early winter (for ice conditions with ice thickness less than approximately 0.5 m) and during the first part of the melt season (May/June).

The correlation coefficients between ice thickness and ice drift speed at each station are calculated by means of equation (11), and the ice thickness was negatively correlated with the drift speed. The values of the correlation coefficients are approximately from  $-0.10$  to  $-0.14$  during the ice growth season and from  $-0.37$  to  $-0.39$  during the

melting season. The values of the correlation coefficients for ice thickness versus drift speed at the three stations are listed in Table 2. The joint frequency distributions of the ice thickness and the ice drift speed are demonstrated in Fig. 12.

Another key parameter in relation to ice drift is the ice concentration. The ice concentrations for the three different stations are given in Fig. 13b. Visually it is easy to see that the ice velocity and concentrations correlate, the ice concentration increased when velocity decreased in the early winter and opposite when the ice melted. As the figures show some of the summers at station A were ice free, whereas station B did not seem to have ice free summers. An example of ice concentration around the observed stations at December 31, 2016 based on information from the National Oceanic and Atmospheric Administration (NOAA) is illustrated in Fig. 13a. The resolution of the ice concentration data is  $1.0^\circ$  latitude  $\times$   $1.0^\circ$  longitude. Furthermore, the ice concentration has implications with respect to the type and the appearance of the ice types. A concentration of 100% implies that no water is visible and that the floes are frozen together, while a concentration of  $\approx 100\%$ – $90\%$  corresponds to very closed pack-ice, a concentration of  $\approx 80\%$ – $70\%$  implies closed pack-ice, a concentration of  $\approx 60\%$ – $40\%$  means pancake floes that are generally not in contact with each other, a value of  $\leq 30\%$  signifies very open ice, and a value of  $\leq 10\%$  represents open water (Alberello et al., 2020; Leppäranta, 2011; Løset et al., 2006; WMO, 1970)

#### 4.2. Joint variation of wind speed and ice drift speed

The recorded time series show different trends for ice drift speed compared to wind speed in the winter and summer seasons (Figs. 14 and 15). In the winter the ice drift speed was clustered around approximately 2.5% of the wind speed for all ice drift. In the summer we found a bi-linear trend. Ice drift speeds less than about 0.2 m/s was correlated with 2.5% of the wind speed. However, for higher ice drift speeds there seemed to be no correlation to the wind speed.

In the winter season, the thickness of the sea ice presents physical effects on the ice drift motion owing to the inertia forces and rheology properties. The thicker sea ice will increase the values of the ice thickness parameter,  $h_i$ , of the inertia term in equation (3) of the governing equation for the sea ice dynamics (Leppäranta et al., 2012). During the winter season, sea ice is subjected to non-free drift conditions due to physical contact between the floes, which accordingly become confined by the surrounding sea ice. In turn, this generates internal stress. Furthermore, the larger surface area of sea ice during the winter allows the wind to dominate the motion of the sea ice dynamics by increasing the air stress corresponding to the aero dynamic drag force. On the other hand, sea ice behaves as the free drift condition in the summer. It tends to drift faster during melting. Reduction of the ice cover area in summer season loses the internal stress from physical contact between the sea ice. The local water stress can provide the local influence on the beneath

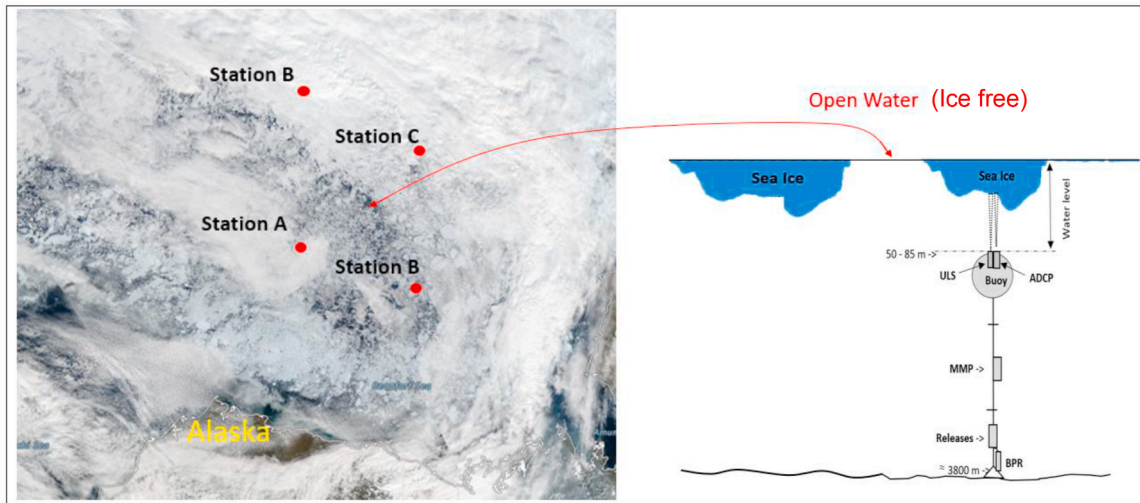
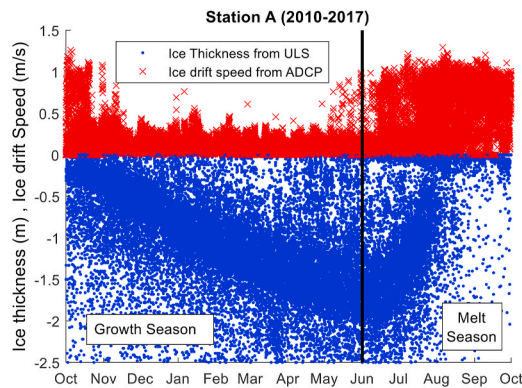
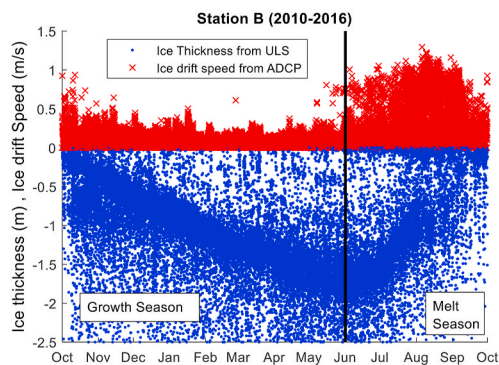


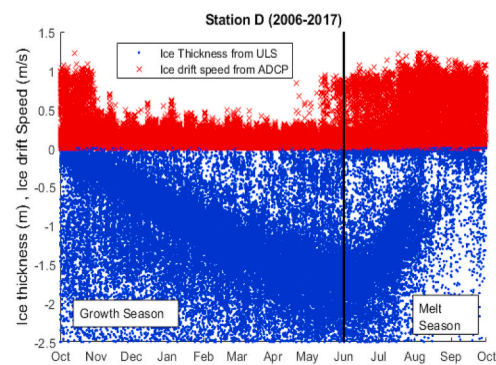
Fig. 10. The presentation of an open water from Satellite image around the observational area in melt season on August 1, 2015.



(a) Ice thickness and ice drift speed at station A



(b) Ice thickness and ice drift speed at station B



(c) Ice thickness and ice drift speed at station D

Fig. 11. The joint variation of ice thickness and ice drift speed at the three stations.(The values of ice thickness refer from the water line).

of ice floats. It can increase the ice drift speed if the water current and the wind blowing have the same direction.

In order to estimate the relationship between the wind and ice drift speed, the scatter data for the ice drift speed and a percentage of the wind speed are fitted to linear regression lines for the winter and summer seasons as illustrated in Fig. 15. For the winter season, the relationship between the ice drift speed and the wind speed seems to follow a linear trend for both station A and D. The percentage of the wind speed

(vertical axis) is adjusted until a slope of 1.0 for the regression line is achieved as shown in the two left parts of the figure.

For the summer season, there are rather different trends for low versus high drift speeds. The percentage of the wind speed (vertical axis) in the low speed range is adjusted until a slope of 1.0 for the regression line. For the high speed range, the sea ice drifts faster than 2.5% of the wind speed above 0.15 m/s for station A and D respectively. A bi-linear fit is applied to the scatter data as shown in Fig. 15. Examples of joint

**Table 2**  
Correlation coefficients between the ice thickness and the drift speed during the winter and summer seasons.

Station	Correlation Coefficients	
	Winter Season (Growth Season)	Summer Season (Melt Season)
A	-0.37	-0.14
B	-0.39	-0.13
C	-0.37	-0.10

frequency distributions between 2.5% of the wind speed and the ice drift speed during the winter and summer seasons is illustrated in Fig. 16.

4.3. The relationship between the ice rose diagram and 2.5% wind rose diagram

In the present study of the Beaufort Sea, the wind data from the NOAA Physical Sciences Laboratory (<https://psl.noaa.gov/data/gridded/data.ncep.reanalysis.pressure.html>) (which provides daily data of the wind velocity expressed in terms of the latitude and longitude components), was applied to generate the wind rose diagram

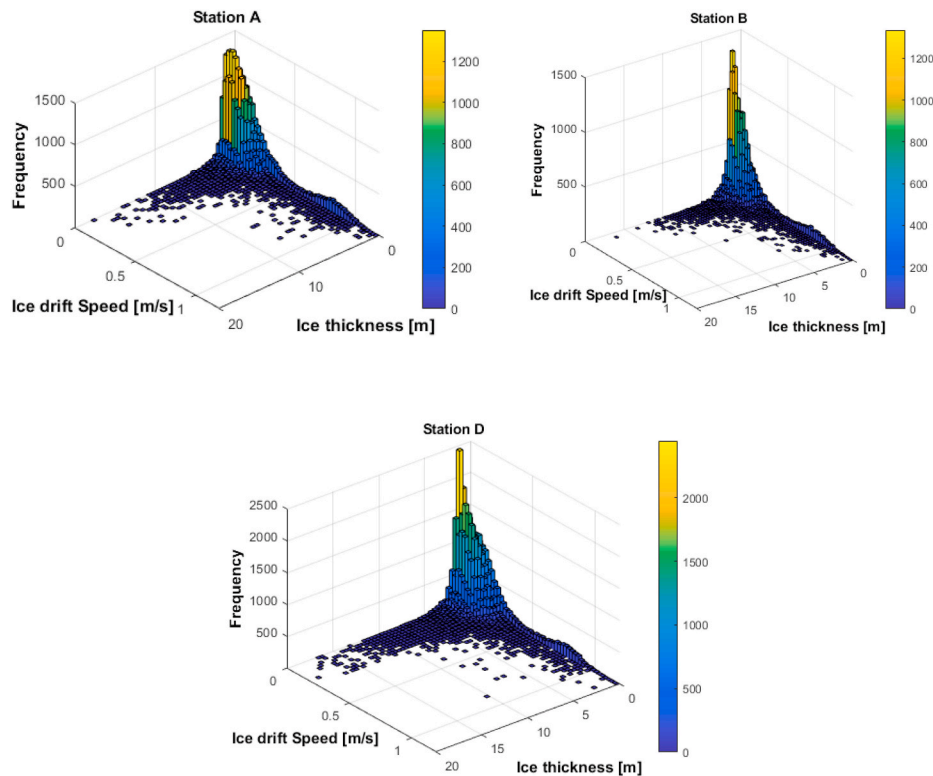


Fig. 12. A joint frequency distribution for the ice thickness and the ice drift speed for each station. (Bin widths of histograms for joint distribution are 0.2 m and 0.02 m/s for ice thickness and ice drift speed).

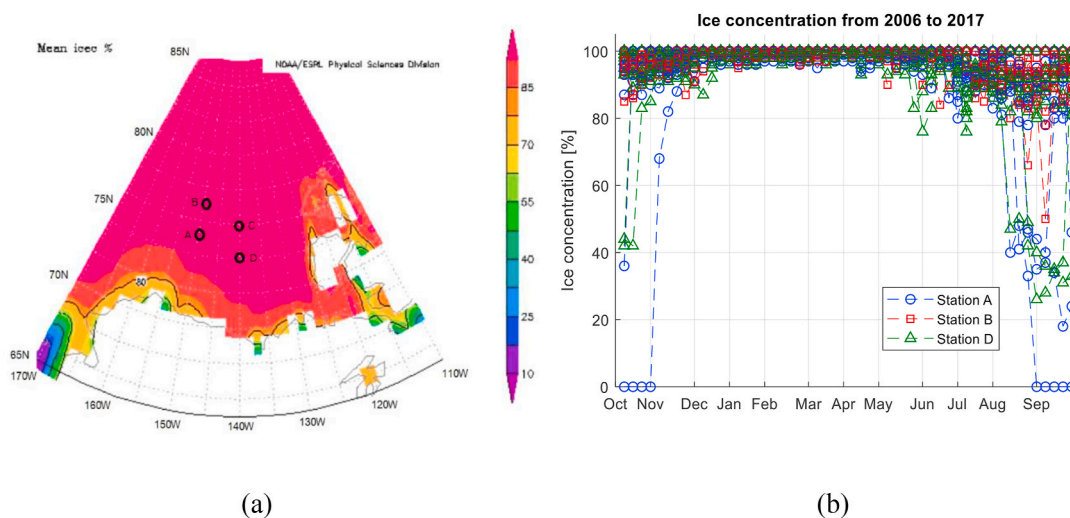


Fig. 13. a) Example of the ice concentration in the Beaufort sea around the observed stations in Dec 31, 2016, b) Weekly mean values of ice concentration at three stations in the Beaufort sea (Source: <https://www.esrl.noaa.gov/psd/data/gridded/data.noaa.oisst.v2.html>).

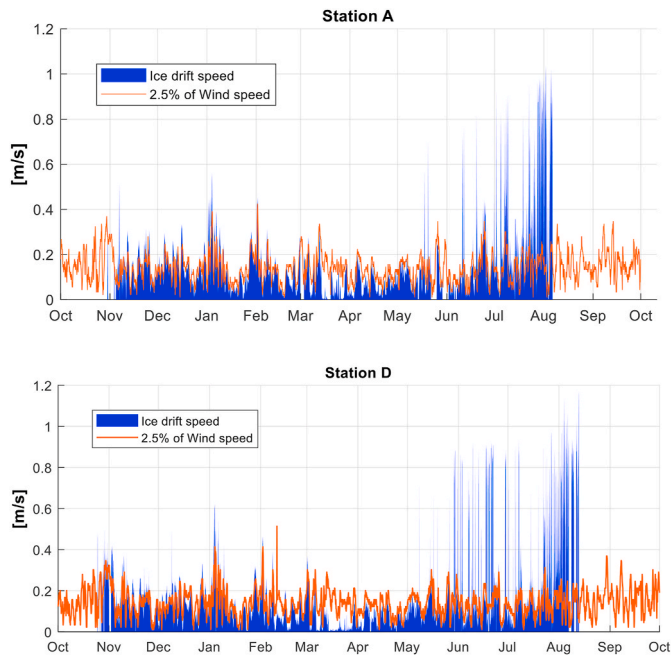


Fig. 14. Time series of ice drift speed and 2.5 percent of the wind speed during 2016–2017 for station A (upper graphs) and D (lower graphs).

corresponding to 2.5% of the wind speed in order to compare with the ice rose diagram. The wind rose diagram for the 2.5% wind speed and the ice rose diagram corresponding to the growth season and the melt season for station B during 2015–2016 is illustrated in Fig. 17. The boundary layer parameter and the Rossby number:  $R_o = V_h(t) / (f \cdot H)$

imply the wind-driven ice drift angle in the rose diagram, where H signify the Heaviside function of ice thickness scale. A low Rossby number indicates that the system is heavily influenced by Coriolis forces, which cause the deviation angle to grow. Here we can see that the major spike in the polar histogram for the wind direction and the ice drift direction has a deviation angle during the growth season of approximately  $20^\circ$ . Due to physical contact, the growth season usually entails non-free drift circumstances. The ice’s motion is restricted as a result of the internal stresses. However, rising ice thickness and clustering sea ice reduce the value of the Rossby number, which enhances the Coriolis impact. On the other hand, the deviation angle for the major spike in the wind and ice rise histograms decreases to  $11^\circ$  during the melting season (i.e., for free drift conditions) due to reduced ice thickness and increased Rossby number, which lessens Coriolis forces, as shown in Fig. 18. In the case of free drift conditions for the northern hemisphere, the observed global deviation angles ( $0 \leq \theta = 11^\circ \leq 30^\circ$ ) correspond with the rule of thumb for the deviation angle of geostrophic wind relative to the ice drift direction (Leppäranta, 2011).

For the winter season, the drifting directions of the sea ice in the ice rose diagram are seen to be in the East-South and North-West direction. Instead, the major direction of the wind rose diagram is towards the East. For the melting season, the wind rose diagram and the ice rose diagram have more or less the same shape.

#### 4.4. Ice rose diagram

ADCP measurements of ice cover drift at each station can be performed in order to generate seasonal ice rose diagrams (Sinsabvarodom et al., 2019). The ice rose diagrams for the growth and melting seasons are shown in Fig. 19. The shapes of ice rose diagrams comply with those of the corresponding mixed Von Mises distributions in polar coordinates. The spokes of the ice rose diagram represent the percentage of drift

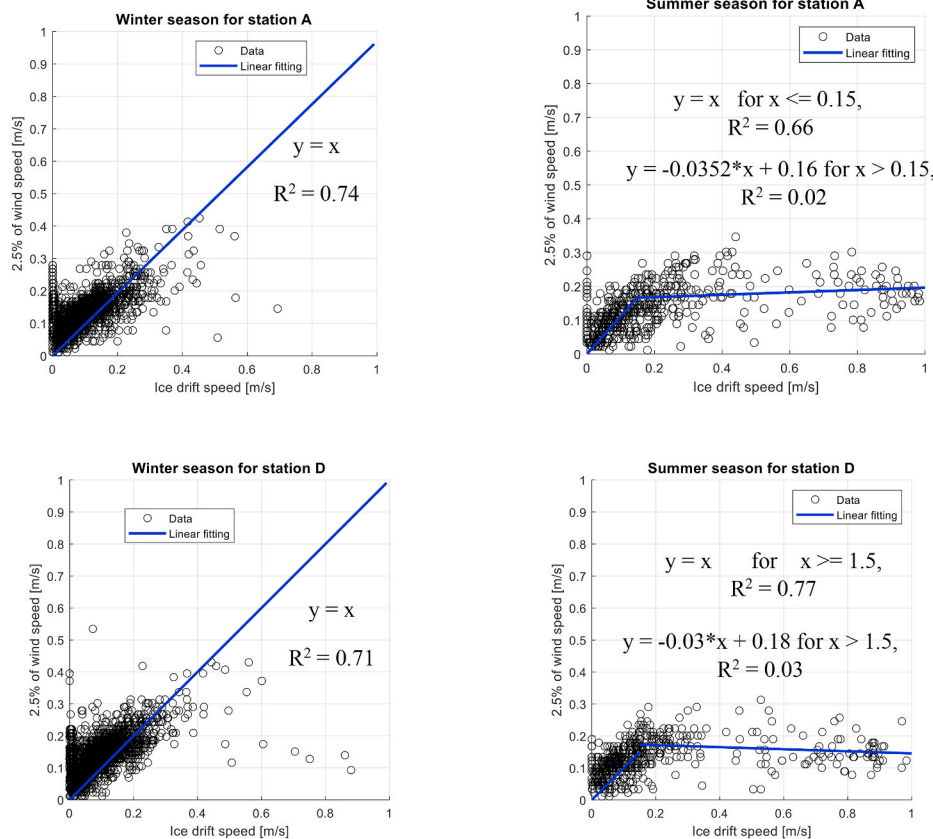


Fig. 15. Comparison of ice drift speed and wind speed during the winter and summer seasons for station A and D.

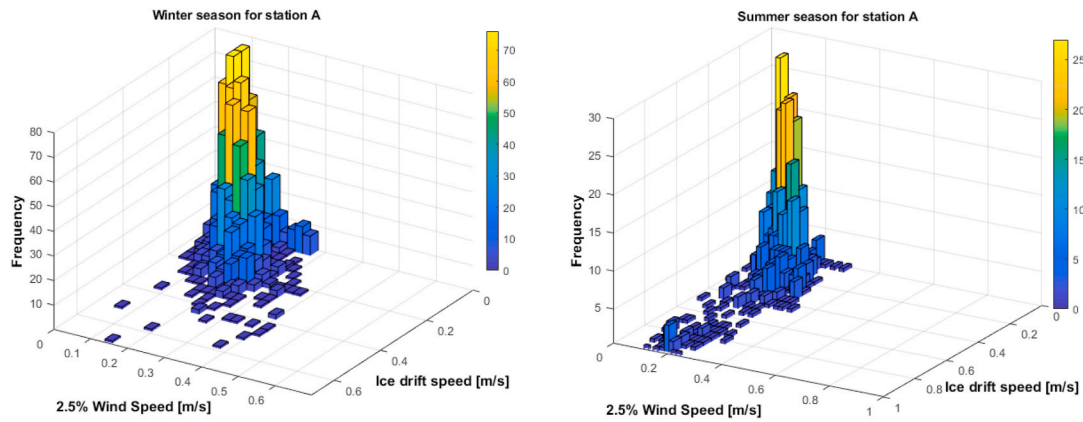


Fig. 16. Examples of joint frequency distribution for 2.5% of the wind speed and the ice drift speed during winter and summer seasons for station A. (Bin widths of histograms for joint distribution are 0.05 m and 0.05 m/s for 2.5% wind speed and ice drift speed).

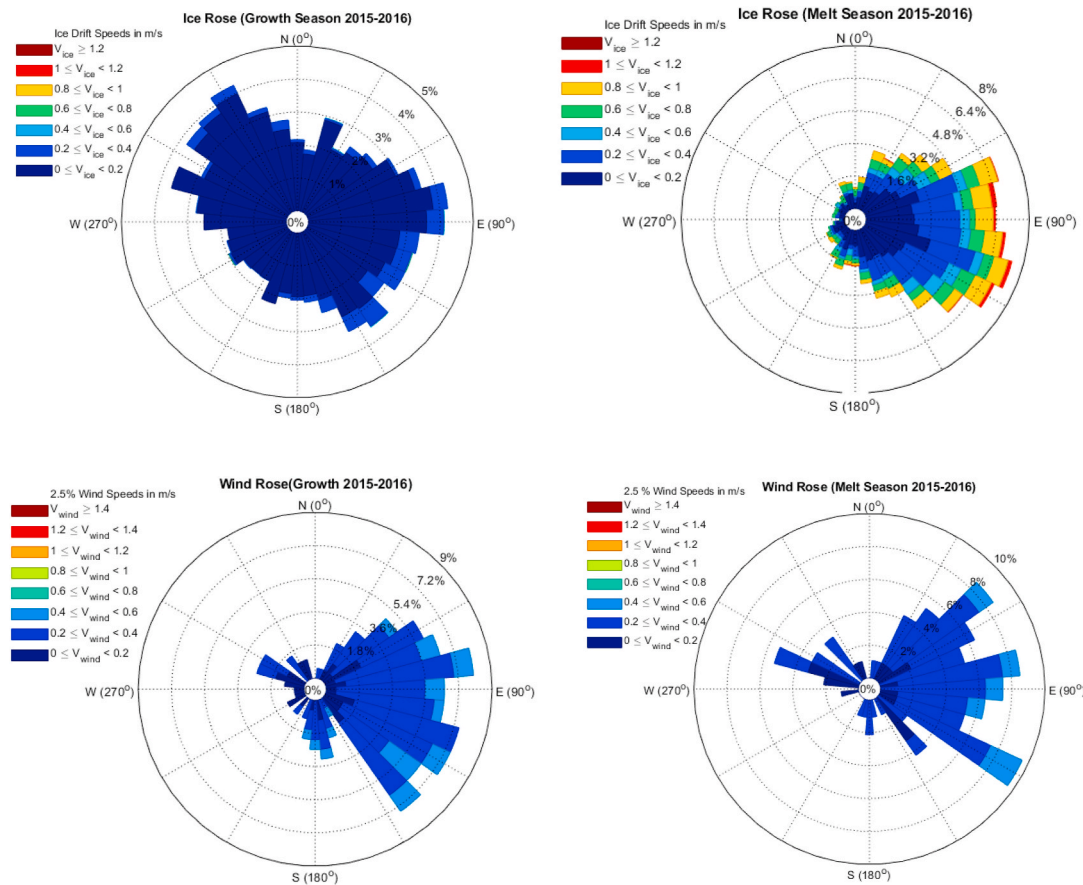


Fig. 17. Ice rose diagrams and Wind rose diagrams during growth season and melt season for station B during 2015–2016 (10° for each bin).

events in each direction. The drift speed is indicated in terms of color contours in the rose diagram. The ice rose diagram is compatible with representation by means of the Eulerian approach, for which the drift speed magnitude and direction as referred to a fixed point in space.

For station A, sea ice tends to drift in the west direction during the growth season, while it moves both in the west and east directions during the melting season from 2010 to 2017. For station B, the majority of sea ice drifts in the east direction both during the growth and melting season for the period 2010–2016. For station D, drift of sea ice is dominantly in the west direction during the growth season, while it moves in the west-south direction during the melting season from 2006 to 2017. At all stations, the sea ice tends to drift with the highest speed

during the melting season, which can be explicitly observed from the color contours of the drift speed in the right-hand side of the picture at each station.

#### 4.5. Probabilistic assessment

Various types of probabilistic models such as the Normal distribution, the Log-normal distribution, the Weibull distribution, the Gamma distribution and the Exponential distribution, have been applied as candidates in order to fit the empirical distribution of the ice drift speed at each station during the growth and the melt seasons. It was found that the Two-parameter Weibull distribution provides the most appropriate

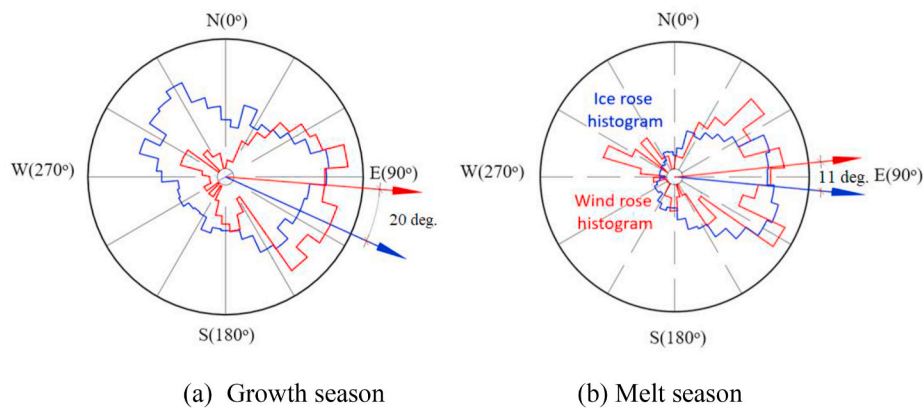


**Fig. 18.** Comparison between directions for the 2.5% Wind rose histogram and the ice rose histogram during the growth season and the melt season for station B during 2015–2016 (The arrow represents the main direction from the origin to the mean value. Each bin is  $10^\circ$ ).

fit for the present data set for the growth season (i.e. for non-free drift conditions). During the summer and the melting season, the sea ice tends to be subjected to free drift conditions especially during the end of the summer season in August. The data of ice drift speed exhibit higher scatter and uncertainty, which can be clearly observed from the recorded time series. The data corresponding to high drift speeds is reflected by the second peak of the probability density function. Therefore, the density function of the ice drift speed can be characterized by two distinct peaks, with one peak at low speeds and one at high speeds. An illustration of the two peak distributions of the ice drift speed is given in Fig. 20.

A mixed distribution is accordingly applied in order to describe this complex behavior for the different drift conditions. The majority of ice drift data corresponds to the leftmost peak of the distribution, which is also reflected by this peak being the highest of the two. Different types of probabilistic model have been considered as the candidates to fit the leftmost part of the distribution. It is found that the lognormal model represents the most appropriate fit for the data set. The second peak of the distribution represents the high drift speeds. The Normal distribution model is found to provide a good fit for this part. The first and second parts of the data are split by the valley between two peaks in order to perform the probabilistic model fitting by application of probability paper for the mixed distribution model. The relative magnitudes of the weight factors for the two distribution types provide information about their relative influence. The PDF components of the mixed distribution and the weight factors of the leftmost PDFs at each station are listed in Table 3.

PDFs and CDFs of ice drift speed at each station during the growth season (i.e. with compact ice conditions) and during the melting season with loose floes are plotted in Fig. 21. During the growth season, the sea ice drifts at lower speeds (due to non-free drift conditions), which implies that the internal stresses play an importance role by converting some of the kinetic energy into deformation of the ice. The mean values of the speed at the three stations are in the range from 0.11 to 0.12 m/s. During the melting season (i.e. with free drift conditions), the internal stresses will diminish owing to the loose ice floes. The mean values of the drift speed increase and are located in the range from 0.2 to 0.3 m/s. Furthermore, during the growth season (i.e. for non-free drift conditions with associated presence of internal stresses), the level of uncertainty associated with the ice drift speed is reduced. This can be observed from the lower values of the standard deviation and the coefficients of variation (COV) as shown in Table 4. The present results match those obtained by Babb (2014) quite well. He has studied the seasonal evolution of ice drift in the Beaufort Sea during 2012. He also found that the mean values of ice drift speed are approximately 0.1 m/s from April to June and 0.19 m/s from July to September.

The mixed Von Mises distribution has been applied in order to fit the

azimuth angles,  $\theta$ , of ice drift direction in equation (2). An optimization method based on the differential evolution algorithm (Punurai and Pholdee, 2018) is applied in order to estimate the parameters of the mixed Von Mises distribution by minimizing the least square errors ( $R^2$ ) (Wang et al., 2012; Zelenko and Lisac, 1994). Examples of the resulting PDF fitting of ice drift direction based on the Von Mises distribution for the growth and melting seasons are demonstrated in Fig. 22. The mixed von Mises distribution of ice drift direction in polar coordinates is illustrated in Fig. 23. Furthermore, it can be observed that the shape of the mixed Von Mises distribution in Fig. 23 implies the shape of the ice rose diagram in Fig. 19, which corresponds to the directional ice drift distributions.

## 5. Discussion

### 5.1. Ice conditions in terms of joint variation of ice drift speed, ice concentration and ice thickness

The ice condition in terms of joint variation of the ice concentration, ice thickness and ice drift velocity was studied. When an ice cover starts to form it grows both horizontally (increasing the ice concentration) and vertically (increasing ice thickness). At some point the ice covers more or less the entire ocean surface, but the thickness continues to grow throughout the season. Figs. 11–13 show the ice velocity, thickness and concentration and show a clear negative correlation between ice drift velocity and ice concentration. The correlation between ice drift velocity and ice thickness seems to be indirect. In the data, the ice thickness tripled between December and May while no change in ice drift velocity can be observed. This argues that effect of the inertia term is smaller than the ice deformation term in the equations of motion for ice drift (i.e. for non-free drift conditions).

During the growth season, sea ice tends to drift with a lower speed than during melting season as exhibited in Fig. 11. There is a positive correlation between ice thickness and ice concentration. An increase of both ice thickness and ice concentration implies an increase of ice volumes, the former by an increase of vertical extension and the latter by an increase in the horizontal direction (Karvonen et al., 2012). This tends to increase the internal stresses within the ice, which in turn leads to the creation of ice ridges. Furthermore, thicker sea ice physically implies a higher resistance owing to the increase of volume, mass and inertia. The level ice thickness from the three measurement stations reaches its maximum value in the period from May to June. Mostly, the ice concentration in the Beaufort Sea at the three measurement stations were higher than 90 percent during the growth season. From the observed data, the ice drift speed tends to be reduced for conditions with ice thickness greater than 0.5 m and ice concentrations above 90 percent during the growth season. In June, the drift speed started to be increased

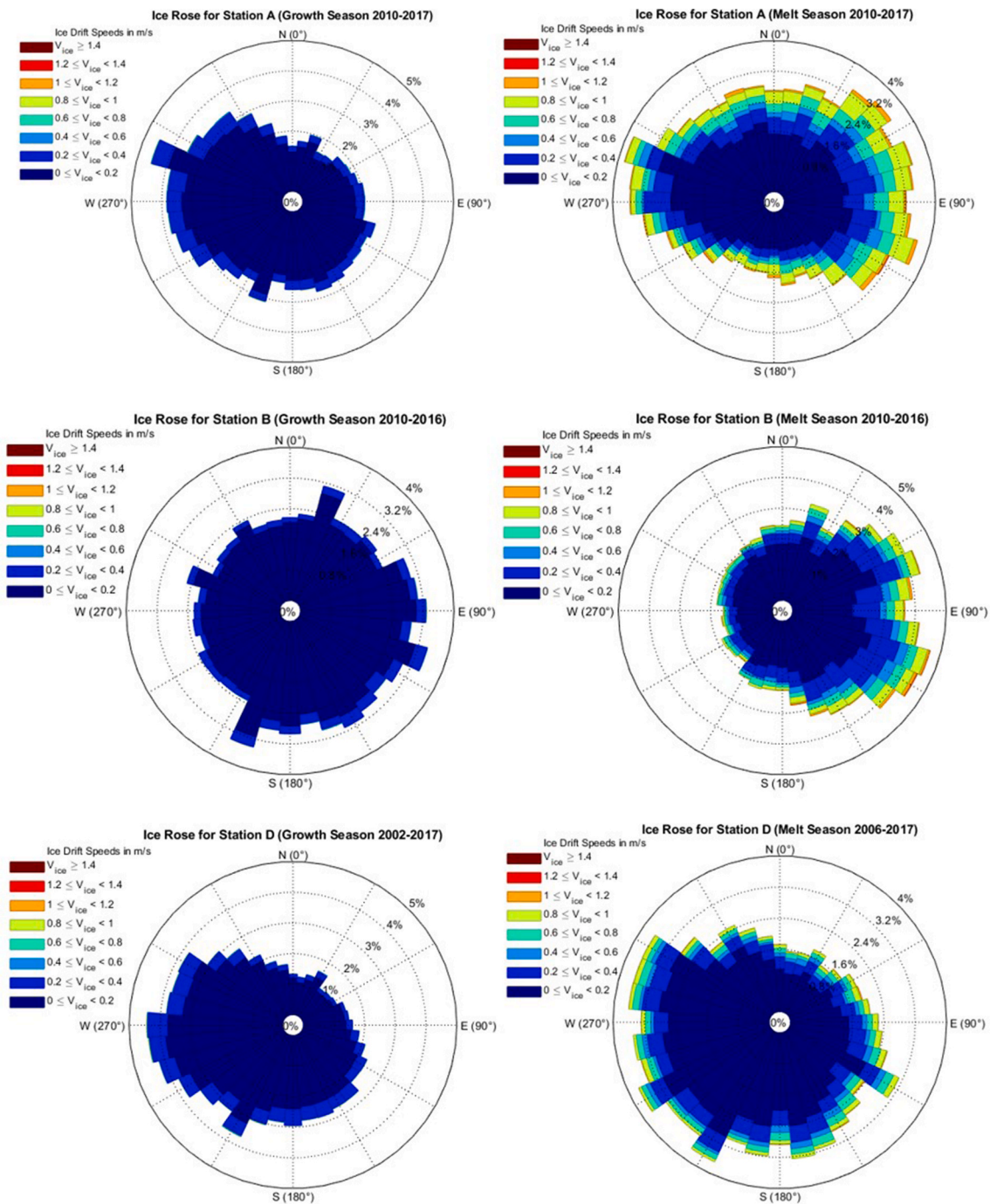


Fig. 19. Ice rose diagrams obtained based on acoustic Doppler current profiler (ADCP) measurements in the Beaufort Sea ( $10^\circ$  for each bin).

significantly when the ice concentration become lower than 90 percent as demonstrated in Fig. 13. The results in the present study also support the conclusion of Spreen et al. (2011) that thinning of the ice cover is likely to cause an increase of the drift speeds. Furthermore, Olason and Notz (2014) found that the drift speed is highest in the middle of August, which supports the present findings.

To give an overall view of the ice coverage during the winter season (i.e. for non-free drift conditions), Fig. 24 shows an aerial view of the sea ice in March. After that, the sea ice can be considered to enter the melting season (i.e. with free drift conditions) as illustrated in Fig. 25, which corresponds to a reduction of ice volumes.

In addition, the joint variation of the ice thickness and the ice drift speed is investigated by computing the correlation coefficient by

application of equation (11). It is found that the correlation coefficient between the ice thickness and the ice drift speed has a negative value as shown in Fig. 12. Furthermore, Hornnes et al. (2020) has studied the joint distribution of the ice thickness and the ice drift speed for the purpose of fatigue assessment at the Norströmsgrund lighthouse in the bay of Bothnia. They found that thicker sea ice tends to drift with a lower speed. In the present study, the joint distribution of the ice drift speed and the ice thickness for each station in the Beaufort Sea is also investigated as illustrated in Fig. 12. The resulting joint distribution of the ice drift speed and the ice thickness in this region is found to exhibit a similar shape as the joint distribution in the Bay of Bothnia. However, the values of the ice thickness in the Beaufort Sea are higher due to the higher latitude with a lower temperature. From the overall shapes of

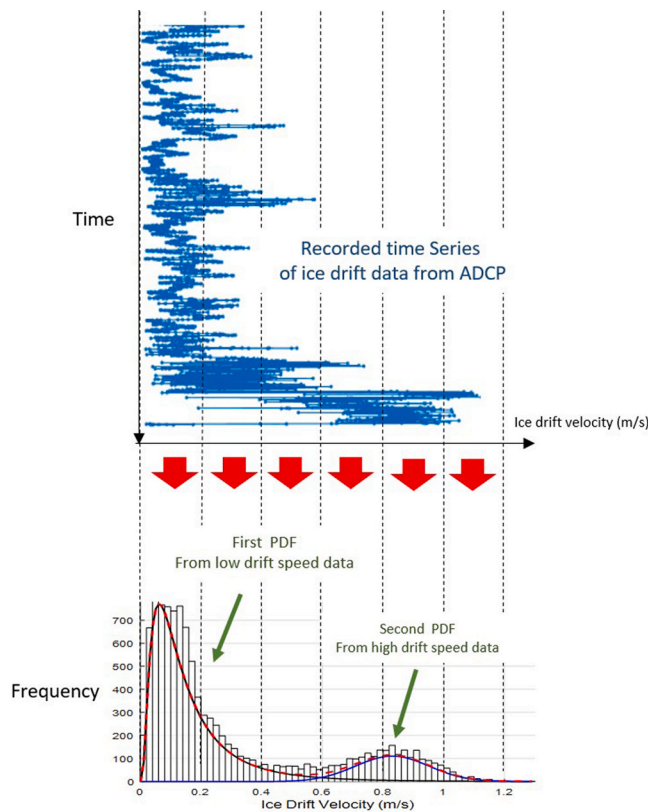


Fig. 20. Example of correspondence between the physical process and the two peak distributions obtained from the measurement time series in summer season.

Table 3

The individual distributions and weight factor for mixture distribution.

Station	First PDF, $f_1(v_h)$		Second PDF, $f_2(v_h)$		Weight factor
	Lognormal distribution		Normal distribution		
	$\mu_1$	$\sigma_1$	$\mu_2$	$\sigma_2$	
A	-2.07	0.77	0.83	0.12	0.81
B	-2.17	0.82	0.81	0.12	0.91
D	-2.27	0.82	0.79	0.11	0.92

histogram for the joint values of the ice thickness and ice drift speed, this supports the foregoing observation that the drift speed is lower for higher values of the ice thickness, which are also typically associated with higher values of the ice concentration.

### 5.2. The relationship between the wind and ice drift

The seasonal wind has a strong influence on the ice drift in the Beaufort Sea. The ratio between the magnitude of drift speed versus wind speed in the Beaufort Sea is somewhat higher than the typical 1–2% wind speed ratio for the Arctic Sea (Spreen et al., 2011). Kawaguchi et al. (2019) also studied the relationship between the wind speed and ice drift speed in the Arctic Ocean at the Northwind Abyssal Plain (NAP) nearby Alaska and found that the magnitude of the ice drift was around 3% of the wind speed. The ratio between the wind speed and ice drift speed from Kawaguchi et al. (2019) is higher than the presently observed 2.5% due to the ocean current flow being in the same direction as the ice drift for that case. This will amplify the ice drift speed.

Our analysis gave a magnitude of the ice drift speed of approximately 2.5% of the wind speed corresponding to a Nansen number of 2.5% (equation (10)). However, the ice drift formulation based on the Nansen

number in equation (10) is simplified by considering only the major external force due to the wind. It neglects many terms corresponding to minor external forces e.g. from water stress and internal stress, Coriolis force, tilting of water surface in the ordinary governing equation of ice drift (Campbell, 1965). In the winter season, the sea ice motion corresponds to the non-free drift condition because of the expansion of the growing sea ice in the horizontal direction, which is reflected by the ice concentration as illustrated in Fig. 13. This implies physical contact and confinement due to the surrounding sea ice. Moreover, the larger surface area of the sea ice cover corresponding to an ice concentration of more than 90% in the winter season increases the area which is exposed to the drag force caused by the wind blowing on the top surface of the ice cover. The non-free drift condition during the winter season is dominated by the global wind. This can be clearly seen from the relationship between the ice thickness, the ice concentration, the ice drift speed and the 2.5% wind speed in Figs. 11, 13 and 14. Conversely, the sea ice motion corresponds to the free drift condition in the summer season. Accordingly, it tends to drift faster during melting which can be clearly seen from the increase of the drift speed when the ice concentrations become less than 90% as illustrated in Figs. 11 and 13. Reduction of the ice concentration implies open water, which can also be seen in the satellite image in Fig. 25. Consequently, reduction of the area of the sea ice cover implies a reduction of the global drag force due to the wind. Therefore, the water stress beneath the ice cover can influence the ice drift behavior to a larger extent. This can increase the ice drift speed to above 2.5% of the wind speed when the forces due to ocean current or the pressure gradient caused by tilting of the water surface are acting in the same direction as the wind is blowing. Furthermore, with wind speeds exceeding approximately 8 m/s (2.5% wind speed = 0.2 m/s), water stress dominates the ice drift speed according to the quadratic drag law and power drag law (Leppäranta, 2011). When the 2.5% wind speed exceeds 0.2 m/s during the summer season, the ice drift speed increases due to the influence of water stress, as shown in Fig. 15.

### 5.3. The relationship between the ice rose diagram and the 2.5% wind rose diagram

The 2.5% wind rose diagram and the ice rose diagram provide exhibit similar trends for the directionality in polar coordinate as illustrated in Figs. 17 and 18. However, the ice rose diagram characteristics in terms of an Eulerian frame description as obtained from the subsurface mooring buoy records exhibit a systematic difference from the directions of the 2.5% wind rose diagram during the winter season. The deviation angle between the ice drift and wind in the rose diagram based on the measurement data is observed to be approximately 20 and 11° in the winter and summer seasons as illustrated in Fig. 18. Because non-free drift conditions are caused by rising ice thickness, the inertia effect associated with these plays a significant role. It lowers the Rossby number, which is related to the ice drift's deviation angle as mass increases owing to the Coriolis force. During the summer, however, the deviation angle decreases, which corresponds to free ice drift conditions. The mass reduction lowers the Coriolis impact while increasing the Rossby number. Nevertheless, according to Leppäranta's assumption of free drift motion, the value of the deviation angle in this analysis is in the range of  $0^\circ \leq \theta = 11^\circ \leq 30^\circ$  (Leppäranta, 2011). Typically, the drift direction of the sea ice on the Northern hemisphere can deviate in the clockwise direction (i.e., "ice drift is to the right from the wind direction") by approximately 0–30° relative to the wind direction at the surface. The deviation angle will be in the counter clockwise direction on the Southern hemisphere (Leppäranta, 2011). The values of deviation angles between the wind direction and the ice drift direction are due to the opposite directions of Coriolis effects for the Northern versus the Southern hemisphere. This effect can also be observed by considering the ice rose diagram and wind rose diagram for different locations. Sinsabvarodom et al. (2021b) also found that the deviation angle between the ice rose diagram and the wind rose diagram is approximately

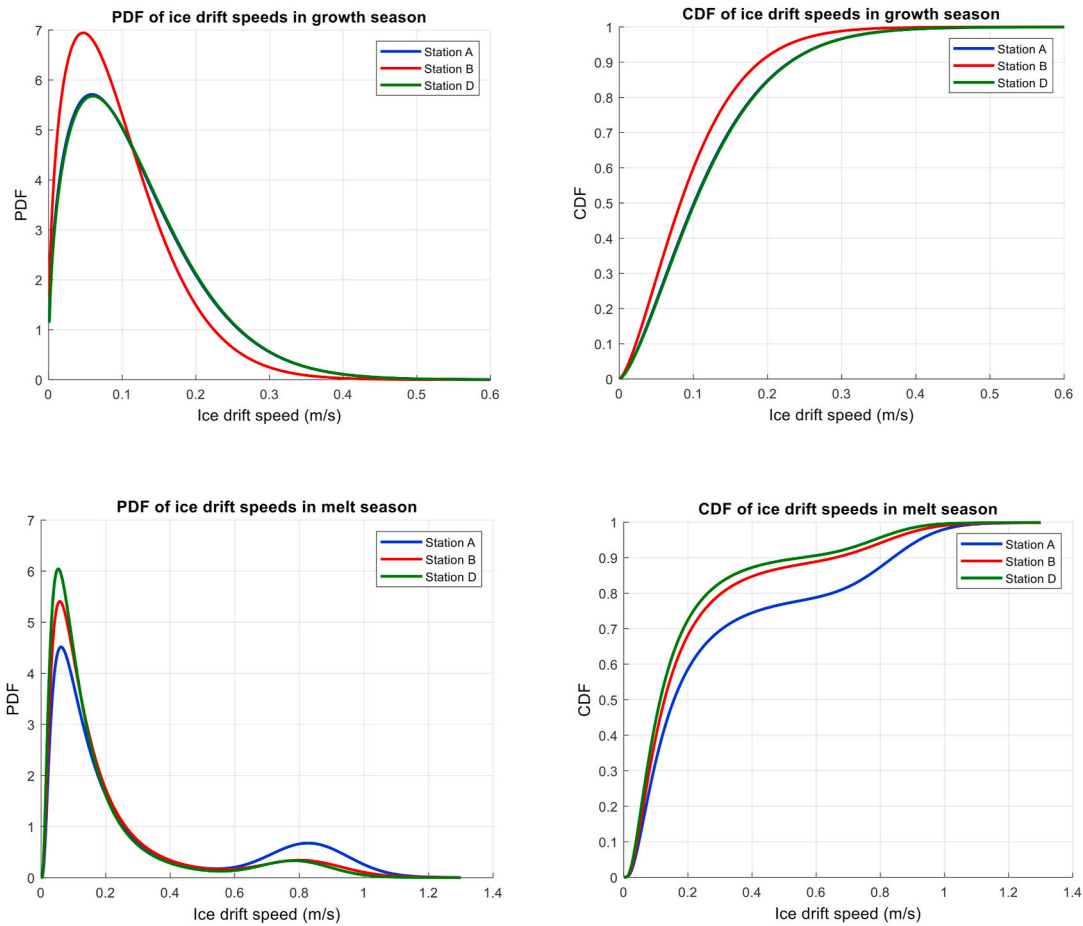


Fig. 21. The PDFs and CDFs of ice drift speeds during the growing and melting season for the years from 2010 to 2017.

**Table 4**  
Statistical data of ice drift speeds (m/s) for growth and melting seasons.

Station	Growth Season			Melting Season		
	Mean Value	STD	COV	Mean Value	STD	COV
A	0.12	0.08	0.67	0.30	0.30	1.11
B	0.11	0.07	0.64	0.23	0.24	1.04
D	0.12	0.08	0.67	0.20	0.22	1.10

30° based on the recorded metocean data based on full-scale experiments in the Bay of Bothnia, which has a sea ice cover only during the winter season.

Furthermore, the ice rose diagrams can be generated based on records of the ice drift. Both the drift speed magnitude and the direction are required in order to generate these diagrams. Where measurements of ice drift speed are not available, numerical weather models providing met-ocean conditions can be utilized in order to predict the ice drift speed and direction. The ice rose diagram can in principle be applied for characterization of drift speed for any ice-covered region of the ocean, and not only the Beaufort sea. For regions with a limited data coverage, it can still be possible to establish ice rose diagrams for short-term ice

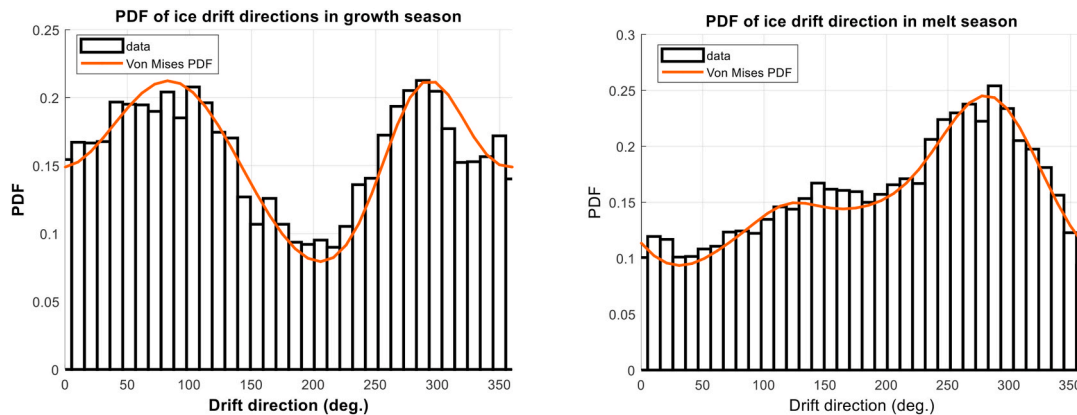


Fig. 22. Examples of PDF fitting by means of the mixed von Mises distribution for ice drift direction at station A from 2010 to 2017.

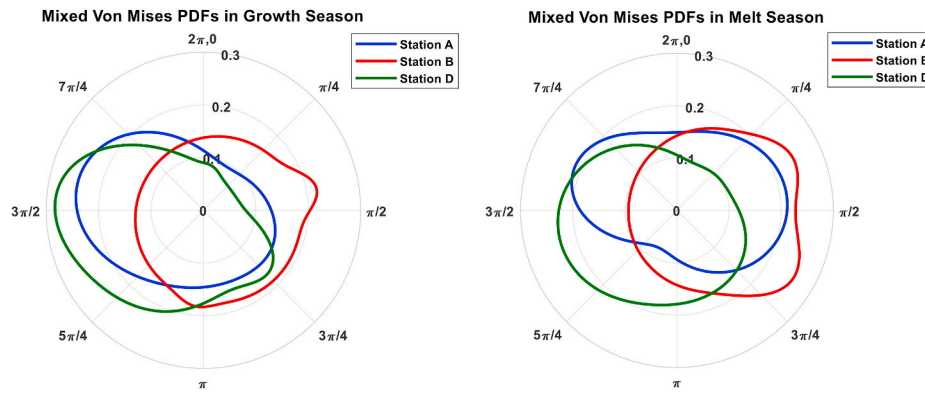


Fig. 23. PDFs of ice drift direction from 2010 to 2017.



Fig. 24. Satellite image of area with observational stations during winter season on March 16, 2015 (<https://zoom.earth/>).

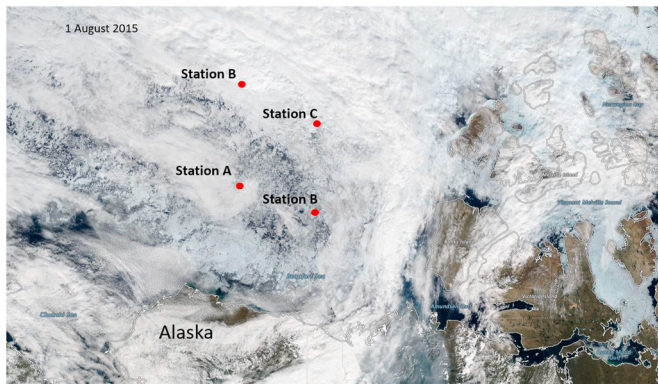


Fig. 25. Satellite image of area with observational stations during summer season on August 1, 2015 (<https://zoom.earth/>).

drift conditions.

## 6. Conclusion

In this work, the ice rose diagram is introduced in order to demonstrate its ability to provide information in relation to ice drift statistics on a compact form, i.e. to convey information both in terms of the percentwise distribution of ice drift magnitude and direction. This information should be of benefit for design of offshore structures at a given sites, both with respect to fixed and floating support structures, also including mooring systems. The ice rose diagram is a generic concept and can be applied in order to characterize the drift speed for any ice-

covered region, not only the Beaufort Sea. This applies not the least to ice rose diagrams which describe the short-term characteristics and hence only require relatively short measurement sequences.

The upward looking sonar (ULS) is beneficial in order to classify data associated with ice cover thickness and for joint recording of relevant velocity data from the acoustic Doppler current profiler (ADCP). These combined records allow estimation of the corresponding ice rose diagram. According to the present study, the following conclusions can be drawn:

- In the Beaufort Sea, the sea ice drifts at a lower speed during the winter (i.e for non-free drift conditions) than during the summer (i.e. for free drift condition), and this seems to be explained by the different characteristics in terms of ice concentrations. In the winter, the ice concentration was mostly far above 0.8 indicating that ice deformation consumed energy and with this reducing the ice drift velocity. The ice concentration also explains the different relationship between ice drift and wind speed in winter and summer.
- According to the probabilistic assessment, the Weibull distribution is found to give the best fit to the present data for the drift speed magnitude during the growth season (which corresponds to non-free drift conditions). For the melting season (which corresponds to free drift conditions), the ice drift speed magnitude data is best fitted by a two peak probability distribution. Mixed distributions based on the lognormal and normal probability models provide the most appropriate fitting. For the ice drift direction, a mixture of von Mises distributions is found to give the best fit to the data.
- The ice drift speed during the winter season in the Beaufort Sea is approximately 2.5% of the wind speed. There is a deviation angle between the ice rose diagram and wind rose diagram less than 30° according to the assumption of the ice drift deviation by Leppäranta (2011). Furthermore, due to the higher ice thickness coupled with the stronger Coriolis force (under non-free drift conditions), the deviation angle is larger during the growth season than during the melt season (with free drift conditions).

Typically, different types of metocean data from field experiments are obtained by different types of instruments with different sampling rates, depending on the physical properties of the instrument and the quantity to be recorded. Furthermore, data processing of the measurements with the objective to estimate the probabilistic characteristics is very important in order to obtain reliable results. Hence, it is also of significant value to study temporal characteristics of the ice conditions in terms of the joint variation of wind, ice drift velocity as well as level ice thickness and ice ridge properties as part of further research.

## Data availability statement

The authors gratefully acknowledge their effort and express our

appreciation for making the measurement data publicly available:

### ULS and ADCP data

The data were collected and made available by the Beaufort Gyre Exploration Program based at the Woods Hole Oceanographic Institution (<https://www2.whoi.edu/site/beaufortgyre/>) in collaboration with researchers from Fisheries and Oceans Canada at the Institute of Ocean Sciences (<http://www.whoi.edu/beaufortgyre>).

### Ice concentration data

The data was published online by National Oceanic and Atmospheric Administration, NOAA(<https://psl.noaa.gov/data/gridded/data.noaa.oisst.v2.html>).

### Wind data

The wind data was available from Ventusky web application, which has been developed by InMeteo company (<https://www.ventusky.com/>). with the wind graphic for each 3 h and 1 h. NOAA Physical Sciences Laboratory (<https://psl.noaa.gov/data/gridded/data.ncep.reanalysis.pressure.html>), which provided the daily wind data with the wind vector in the latitude and longitude direction.

### Satellite images

Available from Zoom Earth, which provides such image in near real-time satellite (<https://zoom.earth/>).

### Funding

This work is supported by the NTNU Oceans Pilot Project Risk, Reliability and Ice Data in Arctic Marine Environments (Project number: 81771037). The second author is now supported by National Natural Science Foundation of China (52201379) and Fundamental Research Funds for the Central Universities (WUT:3120622898).

### CRediT authorship contribution statement

**Chana Sinsabvarodom:** Writing – original draft, Conceptualization, Methodology, Software, Formal analysis, Validation. **Wei Chai:** Writing – review & editing, Supervision, Visualization. **Bernt J. Leira:** Writing – review & editing, Supervision, Visualization. **Knut V. Høyland:** Writing – review & editing, Resources, Supervision, Methodology, Visualization. **Arvid Næss:** Writing – review & editing, Visualization, All authors have read and agreed to the published version of the manuscript.

### Declaration of competing interest

The authors declare that they have no known competing financial interests or personal relationships that could have appeared to influence the work reported in this paper.

### Acknowledgments

This work is supported by the NTNU Oceans Pilot Project Risk, Reliability and Ice Data in Arctic Marine Environments. Moreover, the authors wish to thank Ilija Samardžija for valuable discussions about the ADCP measurements.

### References

Alberello, A., Bennetts, L., Heil, P., Eyras, C., Vichi, M., MacHutchon, K., Onorato, M., Toffoli, A., 2020. Drift of pancake ice floes in the winter Antarctic marginal ice zone during polar cyclones. *J. Geophys. Res.: Oceans* 125 (3), e2019JC015418.

Babb, D., 2014. Sea Ice Motion within the Beaufort Sea. Master Thesis University of Manitoba.

Belliveau, D.J., Hayden, H., Prinsenberg, S., 2001. Ice drift and draft measurements from moorings at the confederation bridge, ice engineering applied to offshore regions. *Proceed. 16th Int. Conf. Port Ocean Eng. under Arctic Conditions* 349–358. POAC.

Birch, R., Fissel, D., Melling, H., Vaudrey, K., Schaudt, K., Heideman, J., Lamb, W., 2000. Upward Looking Sonar Provides Over-winter Records of Ice Thickness and Ice Keel Depths off Sakhalin, Russia. Technical Paper, ASL Environmental Sciences. Sidney, BC, Canada.

Campbell, W.J., 1965. The wind-driven circulation of ice and water in a polar ocean. *J. Geophys. Res.* 70 (14), 3279–3301.

Carta, J.A., Bueno, C., Ramírez, P., 2008. Statistical modelling of directional wind speeds using mixtures of von Mises distributions: case study. *Energy Convers. Manag.* 49 (5), 897–907.

Hornnes, V., Høyland, K.V., Turner, J.D., Deniz, E., 2020. Combined Distribution of Ice Thickness and Speed Based on Local Measurements at the Norströmgrund Lighthouse 2000–2003. 25 Th IAHR International Symposium on Ice.

Karvonen, J., Cheng, B., Vihma, T., Arkett, M., Carrieres, T., 2012. A method for sea ice thickness and concentration analysis based on SAR data and a thermodynamic model. *Cryosphere* 6 (6), 1507–1526.

Kawaguchi, Y., Itoh, M., Fukamachi, Y., Moriya, E., Onodera, J., Kikuchi, T., Harada, N., 2019. Year-round observations of sea-ice drift and near-inertial internal waves in the Northwind Abyssal Plain, Arctic Ocean. *Polar Sci.* 21, 212–223.

Leppäranta, M., 2011. The Drift of Sea Ice. Springer Science & Business Media.

Leppäranta, M., Oikkonen, A., Shirasawa, K., Fukamachi, Y., 2012. A treatise on frequency spectrum of drift ice velocity. *Cold Reg. Sci. Technol.* 76, 83–91.

Li, W., Lam, S., 1964. Principles of Fluid Mechanics, 175–117. Addison-Wesley, Reading, Mass.

Løset, S., Shkhinek, K.N., Gudmestad, O.T., Høyland, K.V., 2006. Actions from Ice on Arctic Offshore and Coastal Structures. Lan, St. Petersburg, Russia.

McPhee, M., 2008. Air-ice-ocean Interaction: Turbulent Ocean Boundary Layer Exchange Processes. Springer Science & Business Media.

McPhee, M.G., 1980. An analysis of pack ice drift in summer. *Sea ice process. Model.* 62–75.

Nansen, F., 1902. The oceanography of the north polar basin. The Norwegian north polar expedition 1893–1896. *Sci. Resul.* 3 (9).

Olason, E., Notz, D., 2014. Drivers of variability in Arctic sea-ice drift speed. *J. Geophys. Res.: Oceans* 119 (9), 5755–5775.

Punurai, W., Pholdee, N., 2018. Optimal structural elements sizing using neural network and adaptive differential algorithm, handbook of research on emergent applications of optimization algorithms. IGI Global 93–134.

Richard, K., Andrey, P., 2006. BGOS ULS Data Processing Procedure. Woods Hole Oceanographic Institution.

Richard, K., Johnson, T., Andrey, P., 2003. BGFE 2003–2004 MMP EMCTD and ACM Data Processing Procedures.

Rossby, C.-G., Montgomery, R.B., 1935. The Layer of Frictional Influence in Wind and Ocean Currents.

Rossiter, C., McKenna, R., 2013. Drift direction changes and implications for sea ice management. *Proceed. Int. Conf. Port Ocean Eng. under Arctic Conditions.*

Shamshiri, R., Eide, E., Høyland, K.V., 2022. Spatio-temporal distribution of sea-ice thickness using a machine learning approach with Google Earth Engine and Sentinel-1 GRD data. *Rem. Sens. Environ.* 270, 112851.

Sinsabvarodom, C., Chai, W., Leira, B.J., Høyland, K.V., Naess, A., 2019. Probabilistic assessment of ice rose diagrams for ice drift in the Beaufort sea. *Proceed. 25th Int. Conf. Port Ocean Eng. under Arctic Conditions.*

Sinsabvarodom, C., Leira, B.J., Chai, W., Naess, A., 2021a. Short-term extreme mooring loads prediction and fatigue damage evaluation for station-keeping trials in ice. *Ocean Eng.* 242, 109930.

Sinsabvarodom, C., Leira, B.J., Chai, W., Naess, A., 2020. Extreme Value Estimation of Mooring Loads Based on Station-Keeping Trials in Ice, ASME 2020 39th International Conference on Ocean, Offshore and Arctic Engineering.

Sinsabvarodom, C., Leira, B.J., Chai, W., Naess, A., 2021b. Probabilistic Fatigue Assessment of a Mooring Line Based on Station-Keeping Trials in Ice, ASME 2021 40th International Conference on Ocean, Offshore and Arctic Engineering. American Society of Mechanical Engineers.

Spreen, G., Kwok, R., Menemenlis, D., 2011. Trends in Arctic sea ice drift and role of wind forcing: 1992–2009. *Geophys. Res. Lett.* 38 (19).

Thorndike, A., Colony, R., 1982. Sea ice motion in response to geostrophic winds. *J. Geophys. Res.: Oceans* 87 (C8), 5845–5852.

Vinje, T., Kvambekk, Å.S., 1991. Barents Sea drift ice characteristics. *Polar Res.* 10 (1), 59–68.

Visbeck, M., Fischer, J., 1995. Sea surface conditions remotely sensed by upward-looking ADCPs. *J. Atmos. Ocean. Technol.* 12 (1), 141–149.

Wang, J., Wang, Z., Yang, C., Wang, N., Yu, X., 2012. Optimization of the number of components in the mixed model using multi-criteria decision-making. *Appl. Math. Model.* 36 (9), 4227–4240.

WMO, 1970. WMO Sea-Ice Nomenclature: Terminology, Codes and Illustrated Glossary. Secretariat of the World Meteorological Organization.

Xu, S., Kim, E., Haugen, S., 2021. Review and comparison of existing risk analysis models applied within shipping in ice-covered waters. *Saf. Sci.* 141, 105335.

Yulmetov, R., Marchenko, A., Løset, S., 2016. Iceberg and sea ice drift tracking and analysis off north-east Greenland. *Ocean Eng.* 123, 223–237.

Zelenko, B., Lisac, I., 1994. On the statistical wind rose analysis. *Theor. Appl. Climatol.* 48 (4), 209–214.